Pergamon

Ann. occup. Hyg., Vol. 40, No. 6, pp. 675–691, 1996

Published by Elsevier Science Ltd. Printed in Great Britain
0003-4878/96 $15.00 + 0.00

PII: S0003-4878(96)00013-0

MAPPING AIR CONTAMINANTS INDOORS USING A PROTOTYPE COMPUTED TOMOGRAPHY SYSTEM

A. Samanta and L. A. Todd*

Department of Environmental Sciences and Engineering, CB #7400, University of North Carolina at Chapel Hill, Chapel Hill, NC 27599, U.S.A.

(*Received* 1 *December* 1995)

Abstract—Single and multiple plumes of sulphur hexafluoride were measured and mapped using a prototype open-path Fourier transform infrared spectrometer (OP-FTIR)–computed tomography (CT) system in an indoor exposure chamber. The OP-FTIR–CT system accurately mapped the position of concentration peaks at different locations in the chamber, and estimated concentrations within a range of 4–50% when compared with point samples measured by gas chromatography with an electron capture detector. Two OP-FTIR spectrometer ray configurations, one with 100 rays and the other with 136 rays, were used to scan the chamber and reconstruct the concentration maps. Ray configuration and time to scan the entire chamber were found to have a profound effect on the quality of the reconstructed maps. The ability to obtain real-time, non-invasive measurements, and to generate spatially and temporally resolved maps of multiple chemicals, makes the OP-FTIR–CT system a promising technique for monitoring source emissions and evaluating exposures to air contaminants in a workplace. Copyright © 1996 British Occupational Hygiene Society.

INTRODUCTION

Current techniques for evaluating exposures in indoor air involve general area and personal sampling. These are essentially point sampling methods and provide concentrations which are spatially limited to the vicinity of a process or worker. The number of samples that are obtained at one time are usually limited; thus, measured concentrations are assumed to be representative of the unsampled regions or unsampled workers in the room. This assumption may not be valid when there are large spatial and temporal variations in chemical concentrations, due to changing ventilation patterns, the movement of people and source emission fluctuations. When integrated sampling methods are used, concentrations are averaged over time, which results in poor temporal resolution; thus, the ability to measure acute exposures is limited. While real-time instruments can be used to provide good temporal resolution of concentration fluctuations, the number of chemicals that an instrument can measure at one time is usually limited.

A new technique is being developed for exposure assessment and source monitoring which provides spatially and temporally resolved estimates of chemical concentrations in work place air. This technique combines the chemical measurement capability of open-path Fourier transform infrared (OP-FTIR) spectroscopy with the mapping capability of computed tomography (CT) to create two-dimensional contaminant concentration maps, non-invasively, and in near real-time.

*Author to whom correspondence should be addressed.

The OP-FTIR spectrometer is an optical remote sensing device that can scan a room and return, in real-time, an integrated concentration over the measured path, not a point sample in one location. Therefore, whether a chemical is located in one place in the optical path or dispersed along the entire path, the spectrometer returns the same average concentration for the entire path. To pinpoint the location of a chemical along a path, a network of overlapping open-path measurements must be obtained. This network can then be processed by a tomographic algorithm to reconstruct a two-dimensional concentration map of an entire room in a few minutes. These maps can be used to provide information about contaminant species and concentrations in the vicinity of workers and sources. When multiple maps are linked together, they can be used to obtain information about contaminant flow patterns for an entire room.

Computed tomography has been used extensively in medicine (Hounsfield, 1973), radio astronomy (Bracewell, 1973) and electron microscopy (DeRosier and Klug, 1968), and was suggested as a method for monitoring air pollution by Wolfe and Byer (1982). The development of this technology for continuous monitoring of indoor air has only recently been explored in simulation studies by Todd and Leith (1990), Todd and Ramachandran (1994a,b) and Bhattacharyya (1995), and in preliminary experimental studies mapping a single peak by Yost *et al.* (1994) and Samanta and Todd (1994).

This paper provides experimental validation of the ability of an OP-FTIR–CT system to map the locations and concentrations of single and double peaks of a single chemical in air, using a prototype OP-FTIR–CT system in a room-size exposure chamber.

THEORY AND METHODOLOGY

Equipment

Experiments were conducted in an exposure chamber that has an exterior wooden structure, is lined with fluorinated ethylene propylene (FEP) Teflon film, and has internal dimensions of $14 \times 12 \times 5.7$ ft ($4.27 \times 3.66 \times 1.74$ m); see Fig. 1. The chamber has a steel mesh floor and an exhaust system that draws air through a plenum in the roof, creating a vertical airflow. A track with two translatable steel tables is located along the interior periphery of the chamber. For these experiments, an 8 in. (20.32 cm) infrared source (I.R.) was mounted on one table and a bistatic Midac OP-FTIR spectrometer (Midac Corporation, Irvine, California, U.S.A.), with a Michelson-type interferometer, with potassium bromide windows and a mercury cadmium telluride (MCT) detector, was mounted on the other table. A 1.75 in. (4.45 cm) dia. telescoping aluminium rod connected the two tables and maintained the alignment of the source and detector. With this set-up, the OP-FTIR spectrometer could be positioned, using a remotely controlled motor, to many different locations in the chamber. Thus, multiple OP-FTIR spectrometers could be simulated using a single spectrometer. The concentration measured by the OP-FTIR spectrometer was divided by the path length (distance between the interferometer and I.R. source), to obtain a path-averaged concentration (ppm).

The chamber was equipped with injection and sampling ports; the injection system consisted of 1/8 in. (0.32 cm) copper tubing, which could be positioned at any

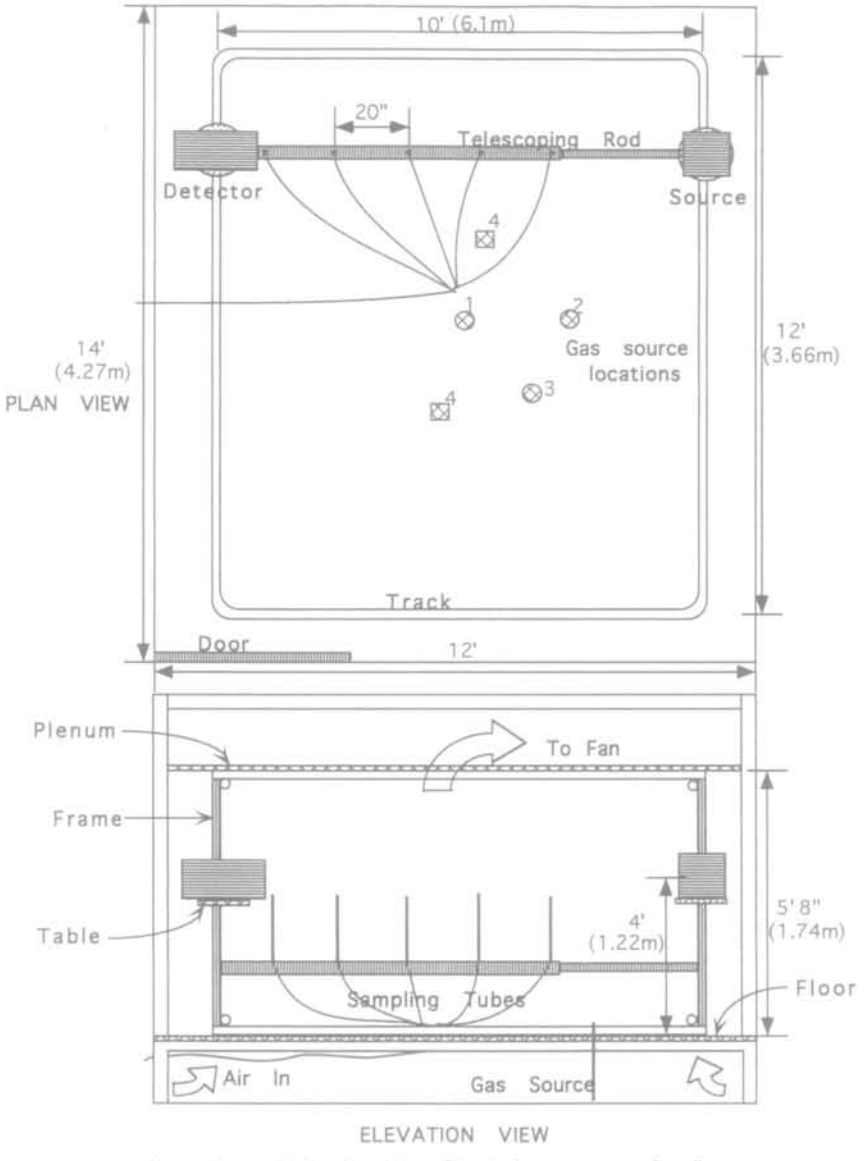

Fig. 1. Plan and elevation view of the indoor exposure chamber.

location (Fig. 1) under the floor of the chamber. Sulphur hexafluoride (SF_6) was used as the tracer gas for all of the experiments. The point sampling system consisted of tygon tubes (3/32 in. or 0.24 cm ID) mounted on the telescoping rod, at the height of the I.R. beam, at 20 in. (50.8 cm) intervals. Gas samples were pulled, using a metal bellows pump (Senior Flexonics Inc, Sharon, Massachusetts, U.S.A.), directly into tedlar bags (Plastic Film Enterprise, Royal Oak, Michigan, U.S.A.). Before collecting a gas sample, the line was flushed out for 10 s at 1 l. min^{-1} (1000 cm^3

min^{-1}). Gas samples were then collected for 1 min; the tedlar bag samples were then injected into an ITI Gas Chromatograph (Burlington, Massachusetts, U.S.A.) with a Valco electron capture detector (Valco, Houston, Texas, U.S.A.) (GC-ECD).

Before each set of experiments, a calibration curve was obtained for the GC-ECD by diluting commercially available (Scott Specialty Gases Inc, Durham, North Carolina, U.S.A.) gas cylinders of 20.3 ppm (±2%) of SF_6 in air. Five concentrations were used to create the calibration curves.

Ray configuration

A configuration consists of a network of optical rays used to measure the path-integrated concentration of chemicals, which is created by the placement of OP-FTIR detectors and I.R. sources in a work place. Two different ray configurations with four sources were used in the experiments, and had 25 rays per I.R. source (a total of 100 rays) (Fig. 2) and 34 rays per I.R. source (a total of 136 rays) (Fig. 3). For the 100 ray configuration, one I.R. source was placed at the centre of each side of the chamber; for the 136 ray configuration two I.R. sources were placed on each of the longer sides of the chamber. Each configuration was composed of rays in a

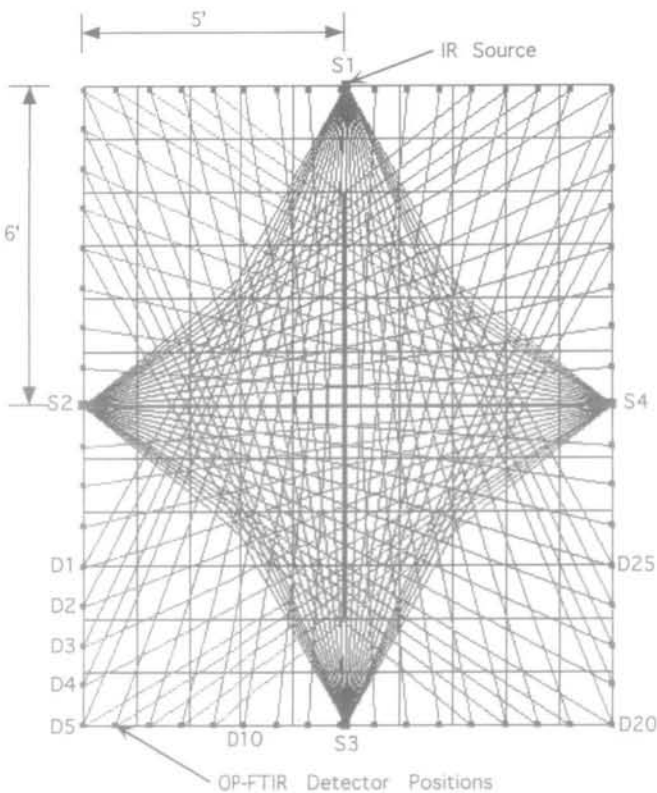

Fig. 2. The 100 ray configuration. The sources are placed at the centre of the sides of the room at positions S1, S2, S3, S4 and the detector is placed at positions D1, D2, ..., D25 corresponding to each source. There are 25 detector positions for each source.

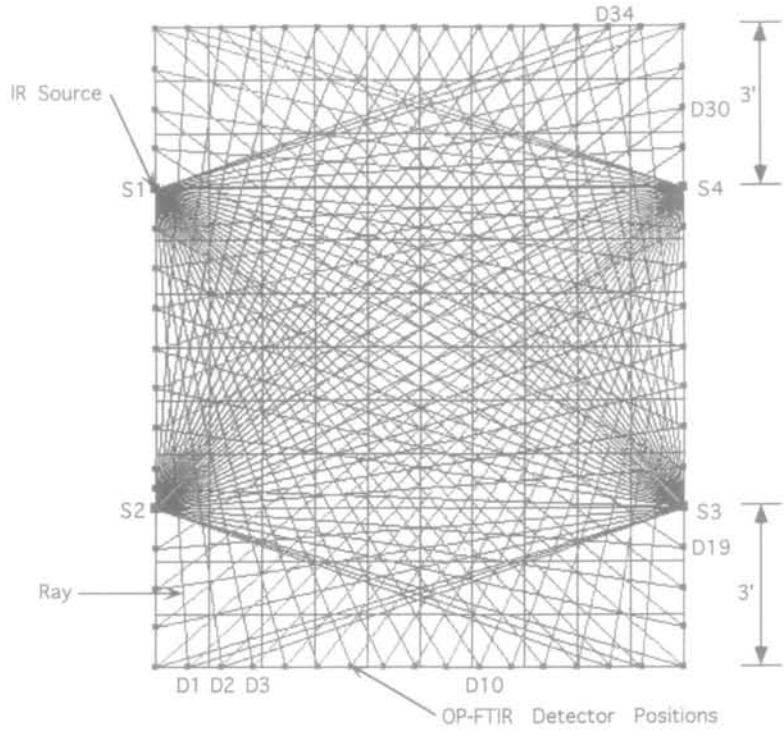

Fig. 3. The 136 ray configuration. There are 34 rays for each source position S1, S2, S3, S4. The detector is placed at positions D1, D2, ..., D34 corresponding to each source.

fan-like arrangement. These were created by pivoting the I.R. sources (S1, S2, S3, S4) about a fixed position and moving the detector along a path around the source (D1, D2, D3, ..., D25); see Fig. 2. An I.R. spectrum was collected at each postition.

Reconstruction algorithms

The path-averaged measurements, referred to as rays, were processed using a tomographic reconstruction algorithm to obtain a two-dimensional concentration map. Although many tomographic reconstruction algorithms have been proposed for other applications, three classes have been explored in the greatest depth: analytic (Cormak, 1963, 1964), back-projection (Brooks and Di Chiro, 1976; Kuhl and Edwards, 1963) and iterative (Hounsfield, 1973; Bracewell, 1956; Gordon *et al.*, 1970). The classes differ in their mathematical foundations, speed and performance under different situations. An iterative method was chosen for this study because iterative methods allow flexibility in the placement of remote sensing equipment in an area, perform well with limited data and allow constraints to be imposed on the reconstructed measurements. These attributes are important for reconstructing chemical concentrations where there are limitations on the quality and quantity of usable data.

An iterative method, maximum likelihood solution using expectation maximization (ML-EM), Equation (1) (Tsui *et al.*, 1991), was selected for this research because reconstructions performed by ML-EM were statistically superior to other iterative

techniques evaluated by Todd and Ramachandran (1994a,b) for the industrial hygiene application.

For the reconstructions, the chamber is first divided into a 10×12 grid of cells; within each cell, the initial concentration, λ_i is assumed to be uniform and positive. At each iteration, ML-EM compares the calculated ray concentrations with the measured ray concentrations, and corrects the values of every grid cell. The correction procedure is shown in Equation (1), and is performed simultaneously for all rays. The correction factor for grid cell i is equal to the sum of ratios of the reprojected value of the grid cell and the backprojected value for the ray, divided by the sum of the weights of the grid cell i for all ray projections. Fifty iterations were used to generate the final reconstructed concentration maps. The CT maps were then converted to a 40×48 grid using bilinear interpolation, to facilitate comparison with GC-ECD point samples. The tomographic maps were generated using Spyglass Transform (Spyglass Inc., Champaign, Illinois, U.S.A.) from the reconstructed concentration data:

$$\lambda_i^{n+1} = \frac{\lambda_i^n}{\sum_j c_{ij}} \sum_j \frac{c_{ij} p_j}{\sum_i c_{ij} \lambda_i^n} \tag{1}$$

λ_i^n = the estimate of image cell i after the n-th iteraton;
p_j = projection data of ray j;
c_{ij} = transfer matrix from image cell i to projection data of ray j;
$c_{ij}p_j$ = the backprojection of projection ray p_j to grid cell i;
$\Sigma_i c_{ij}\lambda_i^n$ = the reprojection of the image estimate λ_i^n.

Point sample maps

Before each set of experiments, repeated measurements were performed, with and without point sampling, to establish that a stable and consistent plume was being generated, and to determine optimum point sampling locations. During each experiment, a total of 30 gas samples was collected from different locations in the chamber. The concentration of each sample was plotted on a 40×48 grid. Point sample maps were then generated by krigging the data using Spyglass Transform. The resolution of the GC-ECD map was 40×48, or four times the resolution of the tomographic maps. This resolution was selected to enable identification of sharp changes in spatial concentrations and to avoid averaging of concentration values over a large area.

Chamber experiments

Before each set of experiments, a blackbody spectrum was obtained; a background spectrum was then collected for each optical ray using 16 co-added scans at 2.0 cm^{-1} wave number resolution. Single or multiple plumes of SF_6 were then generated in the chamber by injecting 5000 ppm of SF_6 in air ($\pm 2\%$) into the chamber from the floor. As the gas was released, spectra were recorded at each detector position using seven co-added scans at 2.0 cm^{-1} wavenumber resolution. While collecting the spectra, point samples from the chamber were collected in tedlar bags and were analysed by a GC-ECD. Each experiment took approximately 1.5 h to complete. At the end of the experiment, Midac Grams/386 software (Galactic

Industries Corp.) was used to quantify each spectrum (930–980 cm^{-1}), using the integration method and comparing the results to a Hanst library spectrum of SF_6 at 0.5 cm^{-1} deresolved to 2 cm^{-1} resolution. The path-integrated concentrations were then processed by the ML-EM algorithm to generate the tomographic concentration maps.

Twenty-two experiments were performed using the 100 ray configuration and 12 experiments were performed using the 136 ray configuration. Twenty single peaks and two sets of double peaks were generated and reconstructed in the experiments which used the 100 ray configuration. Eight single peaks and four sets of double peaks were generated and reconstructed in the experiments which used the 136 ray configuration. Tomographic maps were compared with the point sample maps by comparing the reconstructed location and concentration of the highest concentration point(s) with the known locations and concentrations of the plume(s) of SF_6.

RESULTS

Reconstruction of plume position

In 16 of the 20 experiments conducted using the 100 ray configuration, the OP-FTIR–CT system accurately located the position of single peaks within 1 ft (30.48 cm) (represented by four grid cell for 48×40 grid resolution) of the maximum peak concentration as determined by the GC-ECD point sample map [Figs 4 and 5(a), (b)]. In 17 of the 18 experiments conducted using the 136 ray configuration, the OP-FTIR–CT system accurately located the position of the single peaks within 1 ft (30.48 cm) of the maximum peak concentration as determined by the GC-ECD point sample maps [Figs 6, 7 and 8(a), (b)]. In many reconstructed maps, in addition to the high concentration peak at the plume position, an additional peak (or peaks) was observed at the edge of the chamber.

For reconstructing multiple sources, the 136 ray configuration performed better than the 100 ray configuration. In all the experiments conducted with two plumes and using the 136 ray configuration, the OP-FTIR–CT system accurately located the position of the peaks within 1 ft (30.48 cm) of the maximum peak concentrations, as determined by the GC-ECD point sample map; see Fig. 8(a), (b). In the two experiments performed with the 100 ray configuration, the double peaks were reconstructed in the correct locations; however, there were many artifacts in the corners of the chamber where the ray coverage is limited.

Reconstruction of plume shape and artifacts

While the positions of the plumes were accurately mapped, sometimes there were qualitative differences in the shapes of the plumes mapped by the tomographic and GC-ECD maps. In Fig. 4(a), the OP-FTIR–CT map reconstructed the peak with a broader base than the corresponding sharp peak in the GC-ECD map [Fig. 4(b)]. In Figs 6(a) and 7(a), the OP-FTIR–CT map reconstructed slightly sharper peaks compared to the peaks in the corresponding GC-ECD map [Figs 6(b) and 7(b)]. The maps in Figs 5(a) and 8(a) show artifacts at the edges and the corners of the chamber when compared with the GC-ECD point sample maps [Figs 5(b) and 8(b)]. These artifacts are located in the areas of the chamber that were poorly sampled by the OP-FTIR spectrometer. Despite the observed artifacts, when compared to the GC-ECD

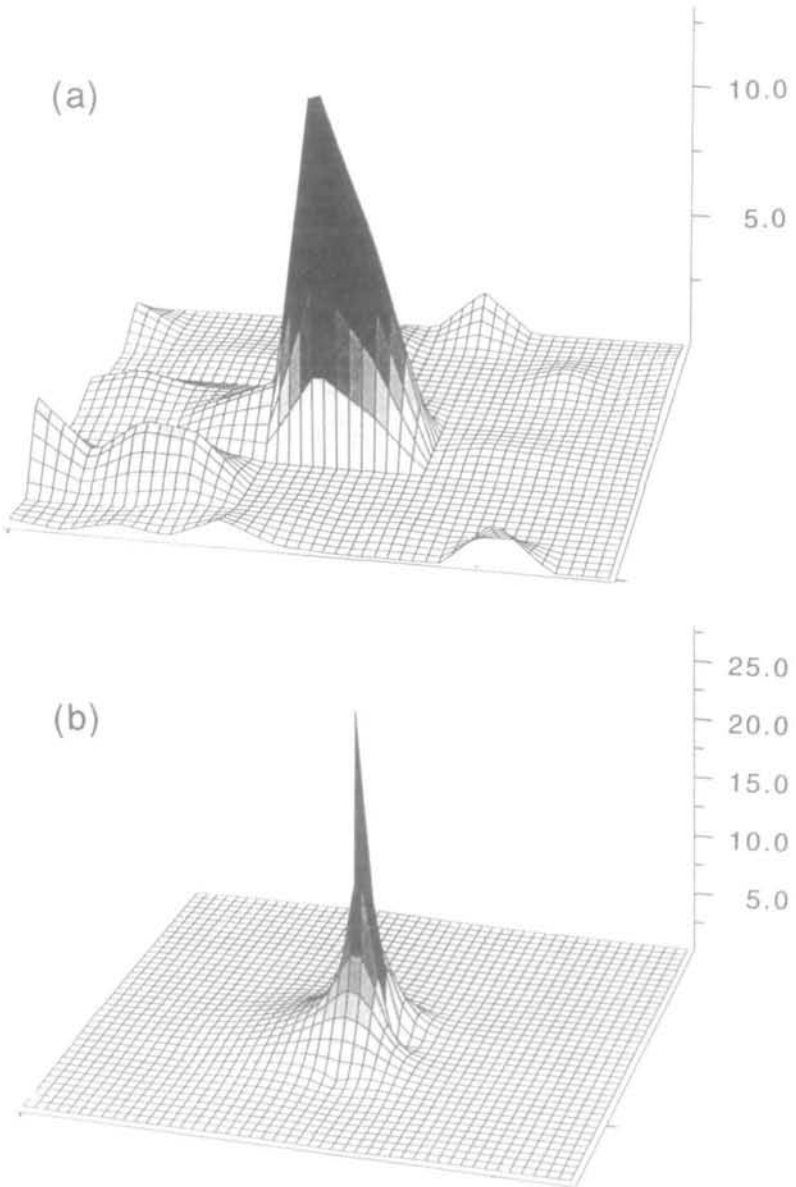

Fig. 4. (a) The computed tomography map for a plume located at position 1, using the 100 ray configuration. (b) The GC-ECD map for the same plume and configuration.

maps, the tomographic maps accurately located the position of highest concentration.

Reconstruction of plume concentrations

In 30 of 34 experiments, the OP-FTIR–CT maps underestimated the peak concentrations compared with the GC-ECD point sample maps; in three

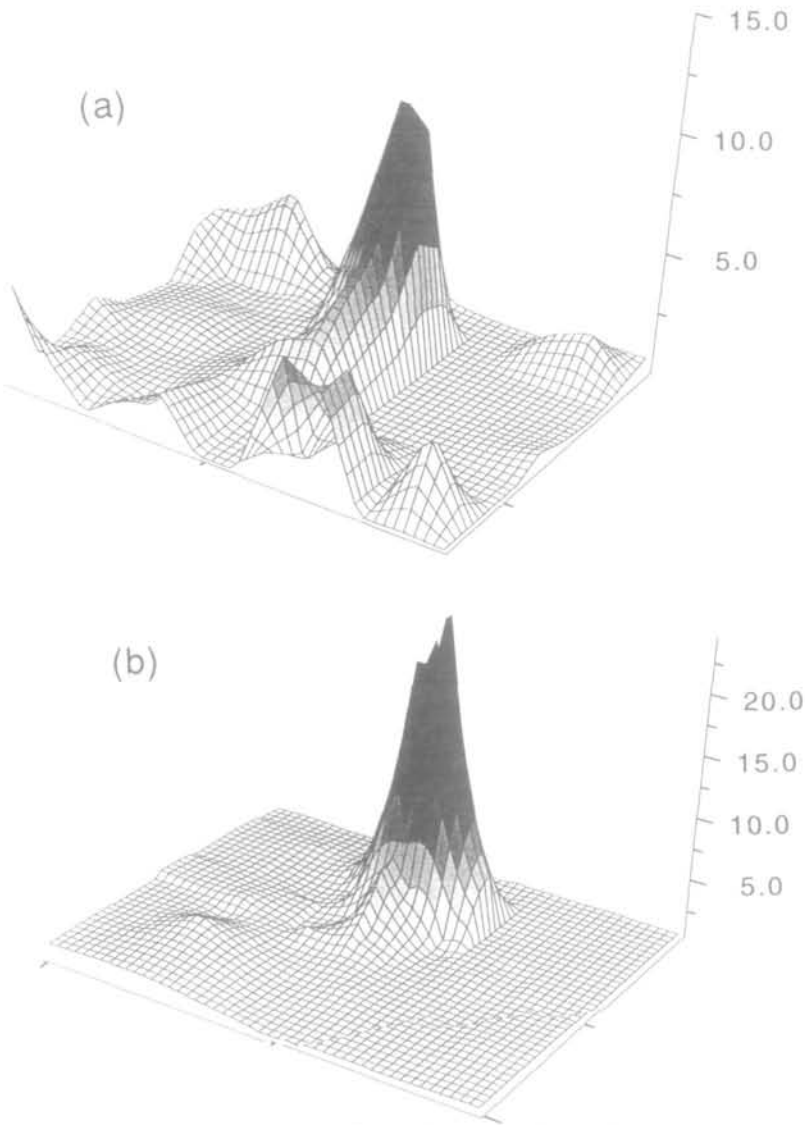

Fig. 5. (a) The computed tomography map for a plume located at position 2, using the 100 ray configuration. (b) The GC-ECD map for the same plume and configuration.

experiments, the tomographic maps overestimated peak concentrations. The peaks were reconstructed within a range of 4–50% (mean = 27%; SD = 18.6%) of the GC-ECD estimated concentrations.

The peak values predicted by the tomographic and GC-ECD point sample maps for five experiments are listed in Table 1. Figures 4(a) and 5(a) are examples of single peaks reconstructed with lower concentrations than the GC-ECD point sample maps. The peak in the reconstructed tomographic map in Fig. 4(a) is 43% lower than the peak in Fig. 4(b); however, it has a broader base than the peak in the GC-ECD

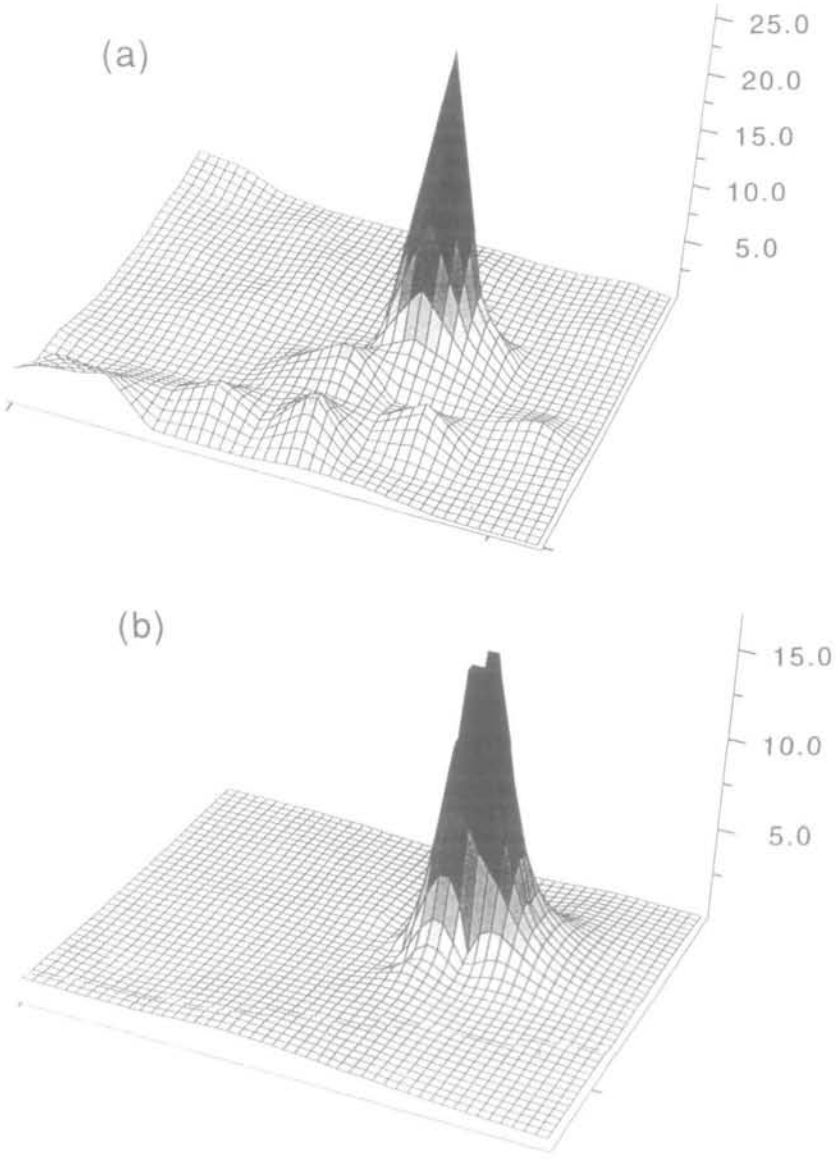

Fig. 6. (a) The computed tomography map for a plume located at position 3, using the 136 ray configuration. (b) The GC-ECD map for the same plume and configuration.

map. Thus, the concentration is spread over a larger area. When the concentrations over 25 grid cells in the 40×48 grid map were averaged, the average concentration for the tomographic map was 9.5 ppm, which is within 12% of the GC-ECD average concentration of 8.5 ppm. In Fig. 5(a), an experiment conducted with the 100 ray configuration, the OP-FTIR–CT system was able to map the position of the source accurately, but the concentration distribution differed considerably from the GC-

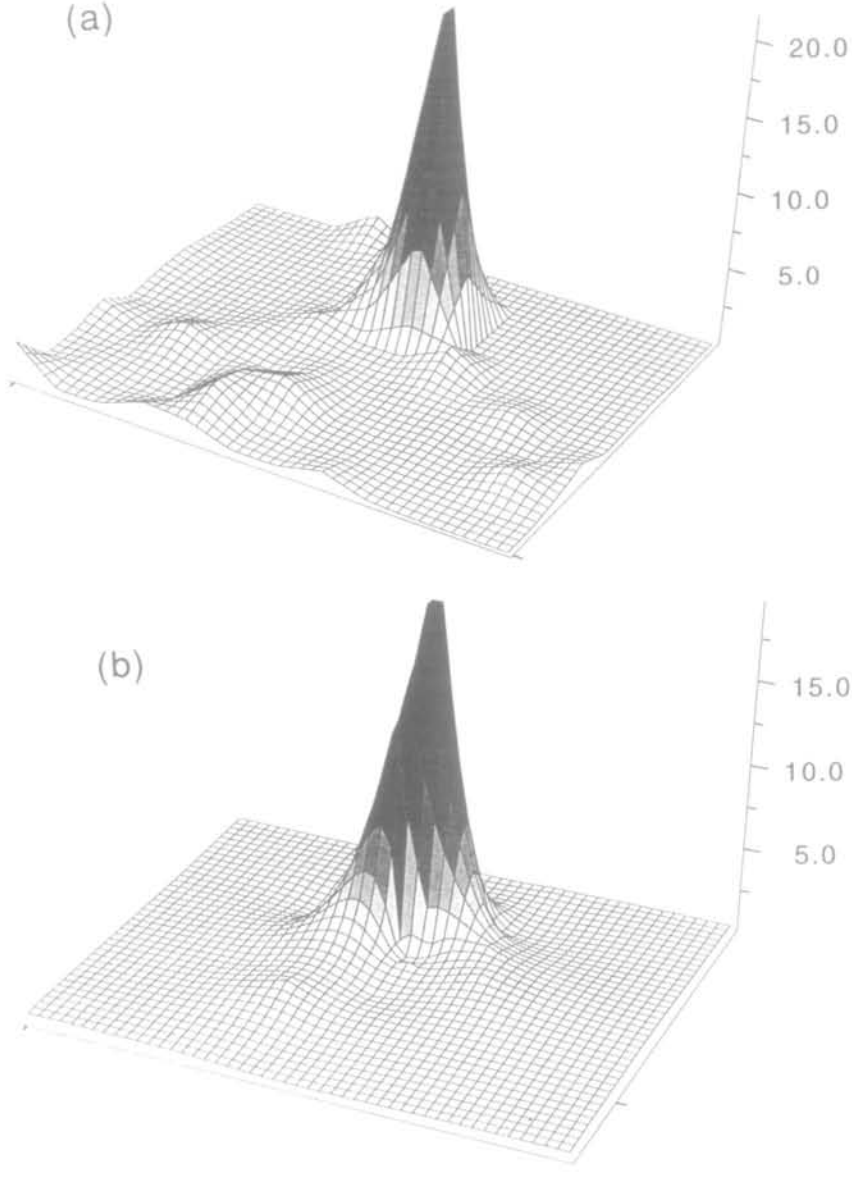

Fig. 7. (a) The computed tomography map for a plume located at position 2, using the 136 ray configuration. (b) The GC-ECD map for the same plume and configuration.

ECD map [Fig. 5(b)]. Compared with the ECD map, the tomographic map [Fig. 5(a)] estimates a plume that has lower concentrations, is spread out, and has artifacts at the edges. In Fig. 8(a), the OP-FTIR–CT reconstructed map concentrations compared quite well with the point sample map concentrations; however, artifacts were observed at the edges of the chamber.

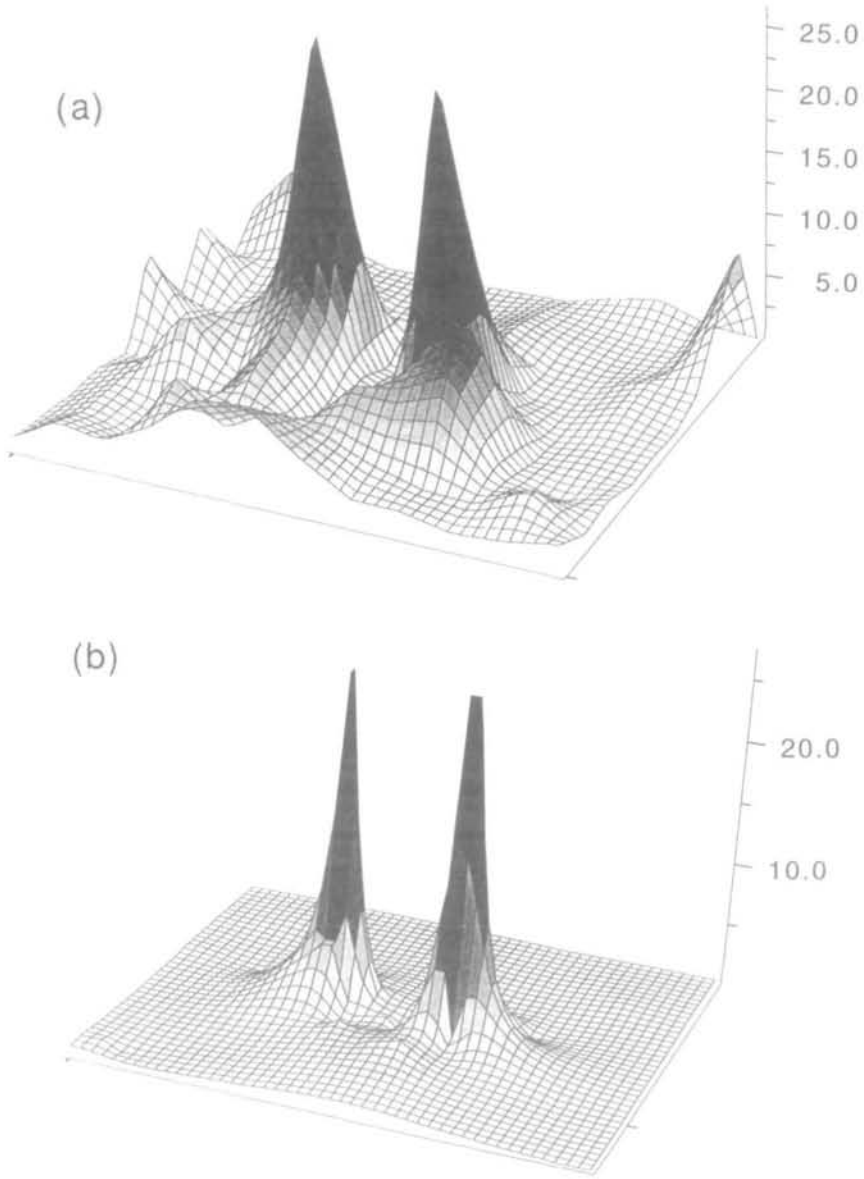

Fig. 8. (a) The computed tomography map for two plumes located at position 4, using the 136 ray configuration. (b) The GC-ECD map for the same plume and configuration.

Figures 6(a) and 7(a) are examples of single peaks reconstructed with higher concentrations than the GC-ECD maps. In Fig. 6(a), the peak is 47% higher than the peak in Fig. 6(b). When 25 pixels around the peak in the OP-FTIR–CT map were averaged, the peak concentration was brought to within 24% of the GC-ECD average. In Fig. 7(a), the OP-FTIR–CT map overestimated the GC-ECD peak concentration by only 10%, and was visually similar to the point sample map.

Table 1. Peak concentrations for GC-ECD analysed and OP-FTIR–CT maps

Fig. No.	Peak location (Fig. 1)	Peak concentration (GC-ECD) (ppm)	Peak concentration (OP-FTIR–CT) (ppm)
4	1	28	16
5	2	25	13
6	3	17	25
7	2	20	22
8	4	Peak 1—27 Peak 2—28	Peak 1—27 Peak 2—27

DISCUSSION

These results show the feasibility of using computed tomography and optical remote sensing to map the location and concentration of indoor air contaminants, non-invasively and in real-time. A prototype OP-FTIR–CT system, which used a single OP-FTIR spectrometer to simulate four spectrometers, was able to accurately pinpoint the location of single and multiple plumes of SF_6 to within 1 ft (30.48 cm). In the majority of the experiments, the reconstructed maps underestimated concentrations.

There are several factors which may have lead to the discrepancies in concentrations estimated by the tomographic concentration maps when compared with the GC-ECD point sample maps. These include: (1) inconsistencies in the ray data due to the slow speed of scanning the chamber; (2) inconsistencies in the point sample data and ray data due to limited and discrete point sampling; (3) inability of the OP-FTIR spectrophotometer or the point samples to consistently sample the true maximum peak concentrations; (4) limitations of the configurations; (5) smoothing of the concentrations by the reconstruction algorithm; and (6) OP-FTIR spectrometer and GC-ECD quantification errors.

The hardware limitations of this study provided the greatest sources of error. The use of only one OP-FTIR spectrometer to simulate four scanning spectrometers, and the time necessary to obtain 30 point samples, resulted in experiments that required approximately 1.5 h to complete. While the vertical flow of the chamber was fairly steady, turbulence was present in portions of the chamber. Therefore, during the experiment, concentrations of SF_6 fluctuated both spatially and temporally. In addition, pulling point samples from the chamber temporarily disturbed flow. Slow scanning of the entire chamber, combined with changes in air flow and plume dispersion, could result in inconsistent ray data, and tomographic maps with inaccurate peak concentrations and artifacts. Although the OP-FTIR–CT system scanned the chamber slowly, peak and average concentrations in the tomographic maps, were in close agreement to the GC-ECD point sample maps.

In this study, the GC-ECD point sample map was considered the gold standard, the true distribution of contaminant in the chamber. This assumption, as was also stated by Yost *et al.* (1994), may not be correct if the plume shifted over time due to changes in airflow. Although 30 point samples were taken throughout the chamber, they were not taken simultaneously. To capture fluctuations in concentrations in real-time, a rapid and extensive point sampling system, capable of simultaneously sampling the entire chamber, would be required. Even if the point sample measured

the maximum peak concentration, the OP-FTIR spectrometer may have sampled the peak at a different point in time and measured a different peak concentration.

When two plumes of SF_6 were injected into the chamber, the number of artifacts in the reconstructions increased. This was probably due to a combination of inconsistent ray sums, as discussed above, and incomplete coverage by the configuration. Computer simulations, which modeled a room with one to six peaks, using four optical sources, resulted in increased peak errors and number of artifacts as the number of peaks increased (Bhattacharyya, 1995; Todd and Ramachandran, 1994a,b). In these studies, the number of artifacts was related to the configuration (number and location of optical sources) and the complexity of the image.

In this study, ray configuration had a significant effect on the quality of the reconstructed concentration map; the 136 ray configuration resulted in better reconstructions than the 100 ray configuration. The two configurations differed, not only in the number of optical rays, but also in the placement of the rays. The 136 ray configuration had better overall coverage of the chamber than the 100 ray configuration and, on average, had more rays hitting each grid cell; see Figs 9 and 10. However, two edges along the shorter dimension of the room were poorly sampled by the 136 ray configuration. This ray configuration could map all the source locations well without many artifacts, and mapped double peaks of SF_6 well; see Fig. 8. The addition of rays, at more angles, in the 136 ray configuration, produced good tomographic maps, despite an increase in the overall scanning time. In simulation

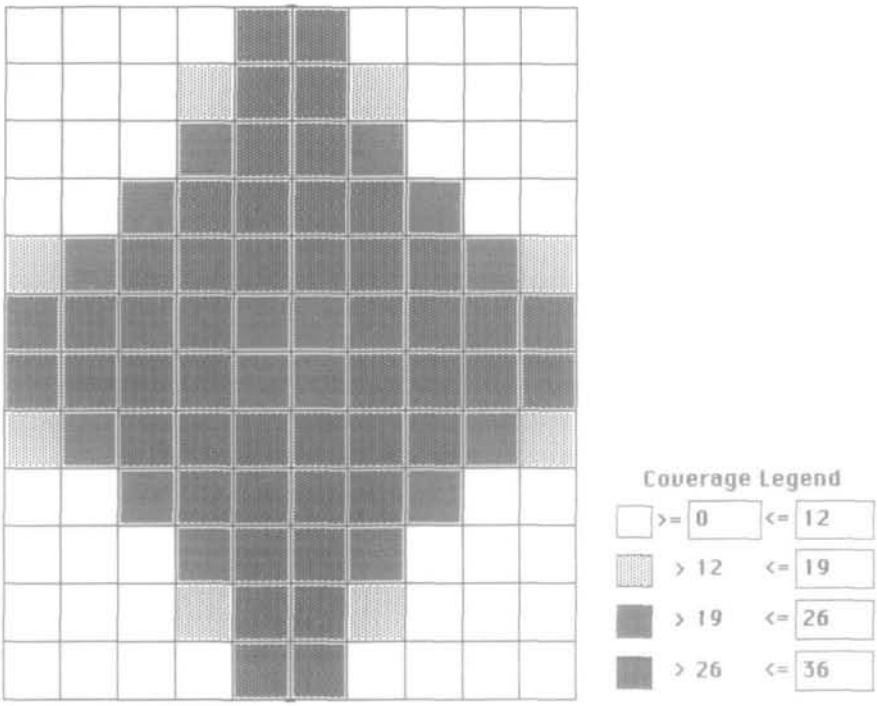

Fig. 9. The ray coverage map, by number of rays sampling a pixel, for the 100 ray configuration.

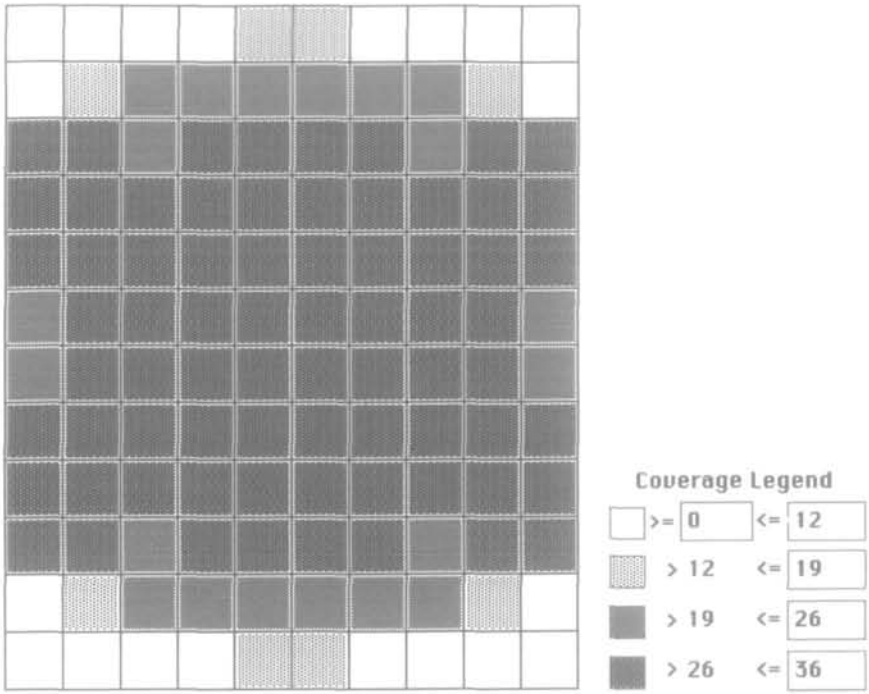

Fig. 10. The ray coverage map, by number of rays sampling a pixel, for the 136 ray configuration.

studies it was observed that at some point the increase in resolution provided by the increased number of rays would be offset by the increase in time, and would result in deteriorated reconstructions. In simulation studies performed by Bhattacharyya (1995), when a plume shifted position and concentration over time, configurations with a large number of rays produced poorer reconstructed concentration maps than configurations with fewer rays, due to increased sampling time.

The 100 ray configuration was able to map SF_6 well, when the plume was located at the centre of the chamber, at location 1; see Fig. 4(a), (b). However, when the plume was located in positions 2 or 3 (Fig. 1) the quality of the reconstruction deteriorated and artifacts were introduced at the edges and corners of the map; see Fig. 5(a). These positions are close to the edges of the room that are poorly sampled, and have few overlapping rays. When grid cells are poorly sampled, artifacts will be introduced into the reconstruction, and peaks will be poorly resolved. Figure 9 shows a map of the number of rays hitting each grid cell in the 100 ray configuration. The grid cells located around the source at location 3 were sampled by fewer rays than the source at location 1.

The tomographic algorithm can introduce errors into the reconstruction; the tomographic technique used tend to smooth out, shorten and broaden concentration peaks. Numerical studies performed by Todd and Ramachandran (1994a,b) to evaluate iterative algorithms for reconstructing concentrations in air, resulted in underestimation of concentrations. The greater the number of optical sources the configuration used, the smaller was the reduction in peak height.

Three other, lesser, sources of error that could have caused discrepancies between the tomographic and point sample maps include: systematic error when quantifying FTIR spectra, error positioning the OP-FTIR system in the chamber when creating the beam positions and systematic errors when calibrating the GC-ECD. Open-path concentrations were not significantly changed, regardless of the quantification method (peak area integration or classical least squares) or the spectral reference library. However, deresolving the 0.5 cm^{-1} library spectra to 2 cm^{-1} introduced up to 3% error in the concentrations. Potential positioning errors were small compared with the dimensions of the chamber.

CONCLUSIONS

This study provides an experimental validation of the ability of an optical remote sensing–computed tomography system to map single and double peaks of a single contaminant in air. The system accurately located the position of the highest concentration points and estimated concentrations within a range of 4–50% when compared with GC-ECD point samples.

These results are promising, given the limitations that the current experimental set-up point sampled the chamber very slowly and that only one OP-FTIR spectrometer was used to simulate configurations with four spectrometers. Non-laminar flow and 1.5 h total scanning time resulted in inconsistent ray data and led to reconstructions with artifacts.

Ideally, a configuration should flood a room with contiguous parallel rays, at many angles, that sample all grid cells identically. In practice, there are many physical and monetary limitations to obtaining a large number of parallel rays. For mapping chemicals in air, the ability to use fewer rays and, thus, fewer optical components is important because it both decreases the cost of the OP-FTIR–CT system and increases the scanning speed. The time to scan a room can also be decreased by decreasing the scanning time for an individual ray; however, this increases the noise in an open-path measurement and raises the lower limits of chemical detection. Alternative configurations are currently being evaluated which scan the room quickly and require fewer rays. A new scanning system is also being developed that can be used without the track; it will rapidly scan the chamber and can be used in an actual indoor environment.

An OP-FTIR–CT system would be a powerful tool for industrial hygienists; potentially, it would provide real-time maps of multiple chemicals in air that are both spatially and temporally resolved. The maps could be used for assessing human exposures to chemicals, leak detection and in ventilation engineering. The non-invasive system could be used over days, weeks or months, and may provide a more accurate assessment of worker exposure to toxic chemicals than are provided by current point sampling methods during short sampling campaigns.

Additional work needs to be performed before this system can be used to qualitatively or quantitatively monitor chemicals in air. Research is currently under way to develop improved OP-FTIR configurations, tomographic algorithms, and OP-FTIR scanning devices. Ultimately, the system must be evaluated in rigorous field studies.

Acknowledgements—The authors acknowledge the funding obtained from the National Institute of Occupational Safety and Health of the Center for Disease Control (grant No. 1 K01 OH00103-01), the U.S. Environment Protection Agency co-operative agreement CR815152 with the University of North Carolina, and the Presidential Faculty Fellow Award of the National Science Foundation (94-53433). Technical assistance obtained from Douglas Norton, Ellen Ward, Shahla Farhat, Keith Latorre and Runa Bhattacharyya in conducting the experiments is greatly appreciated.

REFERENCES

Bhattacharyya, R. (1995) Two-dimensional mapping of air contaminants using an FTIR/computed tomography system: simulation studies. M.S. Thesis, University of North Carolina, Chapel Hill.

Bracewell, R. N. (1956) Strip integration in radio astronomy. *Aust. J. Phys.* **9**, 198–217.

Brooks, R. A. and Di Chiro, G. (1976) Principles of computer assisted tomography in radiographic and radioisotope imaging. *Phys. Med. Biol.* **21**, 689–732.

Cormak, A. M. (1963) Representation of a function by its line integrals, with some radiological applications. *J. appl. Phys.* **34**, 2722–2727.

Cormak, A. M. (1964) Representation of a function by its line integrals, with some radiological applications. II. *J. appl. Phys.* **35**, 2908–2913.

DeRoisier, D. J. and Klug, A. (1968) Reconstruction of three-dimensional structures from electron micrographs. *Nature* **217**, 130–134.

Gordon, R., Bender, R. and Herman, G. T. (1970) Algebraic reconstruction techniques (ART) for three dimensional electron microscopy and X-ray photography. *J. Theor. Biol.* **29**, 471–481.

Hounsfield, G. N. (1973) Computerized transverse axial scanning (tomography). Part I. Description of a system. *Br. J. Radiol.* **46**, 1016–1022.

Kuhl, D. E. and Edwards, R. (1963) Image separation radioisotope scanning. *Radiology* **80**, 653–661.

Samanta, A. and Todd, L. A. (1994) Mapping chemical concentrations indoors using open-path FTIR spectroscopy and computed tomography: chamber studies. In *Proceedings of the Optical Remote Sensing of Environment and Process Monitoring*, pp. 187–191. SPIE, McLean, Virginia.

Todd, L. A. and Leith, D. (1990) Remote sensing and computed tomography in industrial hygiene. *Am. ind. Hyg. Ass. J.* **51**, 224–233.

Todd, L. and Ramachandran, G. (1994a) Evaluation of algorithms for tomographic reconstructions of chemical concentrations in indoor air. *Am. ind. Hyg. Ass. J.* **55**, 403–417.

Todd, L. and Ramachandran, G. (1994b) Evaluation of optical source-detector configuration for tomographic reconstruction of chemical concentrations in indoor air. *Am. ind. Hyg. Ass. J.* **55**, 1133–1143.

Tsui, B. M. W., Zhao, X. D., Frey, E. C. and Gullberg, G. T. (1991) Comparison between ML-EM and WLS-CG algorithms for SPECT image reconstruction. *IEEE Trans. Nucl. Sci.* **38**, 1766–1772.

Wolfe, D. C. and Byer, R. L. (1982) Model studies of laser absorption computed tomography for remote air pollution measurement. *Appl. Optics* **21**, 1165–1177.

Yost, M. G., Gadgil, A. J., Drescher, A. C., Zhou, Y., Simonds, M. A., Levine, S. P., Nazaroff, W. W. and Saisan, P. A. (1994) Imaging indoor tracer-gas concentrations with computed tomography: experimental results with a remote sensing FTIR system. *Am. ind. Hyg. Ass. J.* **55**, 395–402.